Biologically derived melanin electrodes in aqueous sodium-ion energy storage devices

Young Jo Kim[a], Wei Wu[a], Sang-Eun Chun[b], Jay F. Whitacre[a,c,1], and Christopher J. Bettinger[a,d,1]

[a]Department of Materials Science and Engineering, Carnegie Mellon University, Pittsburgh, PA 15213; [b]Department of Chemistry, University of Oregon, Eugene, OR 97403; and Departments of [c]Engineering and Public Policy and [d]Biomedical Engineering,Carnegie Mellon University, Pittsburgh, PA 15213

Edited by Robert Langer, Massachusetts Institute of Technology, Cambridge, MA, and approved November 8, 2013 (received for review July 30, 2013)

Biodegradable electronics represents an attractive and emerging paradigm in medical devices by harnessing simultaneous advantages afforded by electronically active systems and obviating issues with chronic implants. Integrating practical energy sources that are compatible with the envisioned operation of transient devices is an unmet challenge for biodegradable electronics. Although high-performance energy storage systems offer a feasible solution, toxic materials and electrolytes present regulatory hurdles for use in temporary medical devices. Aqueous sodium-ion charge storage devices combined with biocompatible electrodes are ideal components to power next-generation biodegradable electronics. Here, we report the use of biologically derived organic electrodes composed of melanin pigments for use in energy storage devices. Melanins of natural (derived from *Sepia officinalis*) and synthetic origin are evaluated as anode materials in aqueous sodium-ion storage devices. Na^+-loaded melanin anodes exhibit specific capacities of 30.4 ± 1.6 $mAhg^{-1}$. Full cells composed of natural melanin anodes and λ-MnO_2 cathodes exhibit an initial potential of 1.03 ± 0.06 V with a maximum specific capacity of 16.1 ± 0.8 $mAhg^{-1}$. Natural melanin anodes exhibit higher specific capacities compared with synthetic melanins due to a combination of beneficial chemical, electrical, and physical properties exhibited by the former. Taken together, these results suggest that melanin pigments may serve as a naturally occurring biologically derived charge storage material to power certain types of medical devices.

biomaterial | organic electronics | biopolymer | battery

The recent emergence of biodegradable electronics has the potential to transform permanent implantable electronically active biomedical devices into temporary components (1–4). This approach to medical devices can preserve sophisticated capabilities of electronic systems while obviating risks associated with chronic implants (5). Biodegradable electronics devices have been fabricated using a variety of natural and synthetic materials (3, 4, 6–8). However, autonomous on-board power generation remains a significant challenge. Existing power supply strategies include energy harvesting systems or external radiofrequency signals (9, 10). Energy storage devices such as batteries and supercapacitors are used for chronic implants such as pacemakers, neurostimulators, and cochlear implants (11–13). Although high-performance energy storage systems provide a viable solution for temporary implants, toxic electrode materials and organic electrolytes with poor biocompatibility present technical and regulatory hurdles for implementation and clinical adoption of biodegradable implants. Alternative systems that use biocompatible electrode materials with aqueous sodium-ion batteries could provide on-board energy sources for a variety of temporary implantable and edible electronic medical devices (14–16).

There are numerous examples of electrodes that use organic electrolytes for applications in high-density lithium-ion energy storage (17–21). Organic electrodes are advantageous because they can be fabricated into nonconventional device formats that are curvilinear, flexible, and stretchable (22–27). Furthermore, organic electrodes can be prepared using biologically derived materials or biomass toward the goal of achieving sustainable energy storage material production (1, 20). Carbonization of naturally derived materials can produce highly porous materials that exhibit suitable performance for use in primary batteries and supercapacitors (28–30). Anodes have been fabricated using biopolymers including polysaccharides, polypeptides, and cellulosic derivatives (31, 32). Interpenetrating networks of polypyrrole (Ppy) and lignin can serve as renewable cathode materials in energy storage devices (33). The high storage capacity of Ppy/lignin composites is attributed to the redox reactivity of the quinone moieties in lignin combined with the high electrical conductivity of doped Ppy ($\sigma_{Ppy/lignin}$ ~30 S cm^{-1}) (34). Few investigations have used biologically derived materials in sodium-ion energy storage devices for potential use in biomedical applications (35–37). The ideal organic electrode material would be biocompatible or biodegradable and exhibit physicochemical properties to support high charge storage densities. Electrodes should ideally be prepared in a scalable and facile manner to maximize economic viability (38). Biologically derived electrode materials with minimal post-processing are therefore intrinsically advantageous.

Melanins are a broad class of pigments found in many organisms. Melanins are composed of disordered extended heteroaromatic polymer networks (1, 39, 40). Eumelanins are a subclass of melanins that mediate redox reactions and exhibit unique physical properties which are widely used in many important biological functions (41, 42). Eumelanins exhibit unique chemical signatures that can support reversible cation binding including pendant catechols, carboxylates, and aromatic amines (43, 44). Eumelanins exhibit excellent in vitro and in vivo biocompatibility along with biodegradability via free radical degradation mechanisms (8, 45, 46). Furthermore, eumelanins exhibit hydration-dependent hybrid electronic–ionic conduction through self-doping

Significance

Here we present important findings related to biologically derived pigments for potential use as battery electrodes. Namely, we report the synthesis, fabrication, and characterization of melanins as materials for use in aqueous sodium-ion batteries. We demonstrate the use of naturally occurring melanins as active electrode materials in charge storage devices. Furthermore, the performance of melanin anodes is comparable to many commonly available synthetic organic electrode materials. The structure–property relationships that govern the storage capacity in melanin materials were also elucidated. These findings suggest that the unique chemistry and nanostructure in natural melanins increase the charge storage capacity compared with synthetic melanin analogues.

Author contributions: Y.J.K., S.-E.C., J.F.W., and C.J.B. designed research; Y.J.K. and W.W. performed research; Y.J.K. contributed new reagents/analytic tools; Y.J.K., W.W., S.-E.C., J.F.W., and C.J.B. analyzed data; and Y.J.K. and C.J.B. wrote the paper.

The authors declare no conflict of interest.

This article is a PNAS Direct Submission.

[1]To whom correspondence may be addressed. E-mail: whitacre@cmu.edu or cbetting@andrew.cmu.edu.

This article contains supporting information online at www.pnas.org/lookup/suppl/doi:10.1073/pnas.1314345110/-/DCSupplemental.

mechanisms (39) and the ability to form homogeneous nanoparticles that spontaneously aggregate into mesoscale structures with short-range order (47). The unique chemical and physical properties of eumelanins suggest that it can serve as a biologically derived material for use as biocompatible electrodes in high-density charge storage devices. Herein we report the use of biologically derived and synthetic melanin pigments as anode materials for aqueous sodium-ion energy storage devices.

Results and Discussion

Eumelanins are a subset of naturally occurring melanin pigments that are composed of randomly polymerized tetramer units of 5,6-dihydroxyindole (DHI) and 5,6-dihydroxyindole-2-carboxylic acid (DHICA) monomers (40, 48–50). These protomolecules use strong π–π stacking and hydrogen bonding interactions that promote self-assembly into spherical nanostructures with an intermolecular spacing of 3.8 Å and characteristic dimensions of 100–300 nm (50, 51). Synthetic melanins can also be prepared from oxidative polymerization of L-DOPA, dopamine, or indole derivatives (52, 53). Although the chemical functionalities of natural eumelanins are conserved in synthetic melanins, the microstructure is markedly different. Synthetic melanins exhibit morphologies that are dominated by porous networks or dendritic structures as opposed to packed nanoparticle aggregates (47, 54). Three classes of eumelanins were selected to elucidate structure–property relationships in anodes for sodium-ion charge storage devices: (*i*) naturally occurring eumelanins isolated from *Sepia officinalis* (NatMel); (*ii*) synthetic eumelanins prepared from autooxidation of tyrosine (SynMel); (*iii*) synthetic melanin-like materials (E-SynMel) prepared from the oxidative polymerization of 5,6-dimethoxyindole-2-carboxylic acid (DMICA). The resulting spectrum of melanin composition and microstructure can be used to deconvolve the physicochemical signatures as they relate to figures of merit of device performance such as charge storage capacity.

NatMel consists of homogeneous nanoparticle aggregates whereas SynMel and E-SynMel exhibit heterogeneous nanostructures and rod-like microstructures, respectively (Fig. 1 and Fig. S1). NatMel, SynMel, and E-SynMel exhibit Brunauer–Emmett–Teller (BET) surface areas of 19.9, 10.7, and 9.2 $m^2\ g^{-1}$, respectively. The surface areas of all melanins in this study are smaller than many other carbon-based electrode materials (35, 55, 56). SynMel and E-SynMel exhibit hysteresis in N_2 adsorption–desorption isotherms, which suggests that these materials have a mesoscale disorder (57). Conversely, NatMel exhibits higher specific surface areas and reduced hysteresis compared with SynMel and E-SynMel, which suggests that individual NatMel are composed of nanometer-scale textured granules. NatMel and E-SynMel contain smaller pore diameters with narrow distributions compared with SynMel. These quantitative measurements confirm the heterogeneous nanostructure of SynMel that is corroborated by SEM micrographs and elemental analysis (Fig. S2). Increased heterogeneity in SynMel arises as a consequence of the polymerization mechanism.

Eumelanins contain moieties that can reversibly bind multivalent cations through the formation of organometallic complexes (43). Strategic selection of monomers used in SynMel and E-SynMel polymerization permits the deconvolution of the relative contributions of chemical signatures as sodium cation binding sites in NatMel anodes. Catechol groups, present in both NatMel and SynMel, are redox active sites that reversibly bind cations (58–60). NatMel contains electronegative aromatic amines in DHI/DHICA monomers that also bind cations reversibly (48, 61). Pendant carboxylates can also bind monovalent cations through Coloumbic interactions (17). Approximately 75% of the aromatic bicyclic monomers in NatMel contain a carboxylate at the 2 position as measured by X-ray photoelectron spectroscopy (XPS; *SI Text*). NatMel contains DHI, which does not feature a 2-carboxylic acid group, whereas both SynMel and E-SynMel are formed from monomers with carboxylates. Exogenous proteins were not present within biologically derived melanins in significant amounts as determined through Raman and XPS spectra (*SI Text*).

The location of sodium-ion loading within melanins was assessed using XPS (Fig. S3 and Table S1) and Raman spectroscopy (Fig. 2). Peaks in the O (1s) region of the XPS spectra occurred at energies of 533.25, 531.92 ± 0.2, and 530.79 ± 0.3 eV, which are associated with COOH, C–OH, and C–O functionalities, respectively (62, 63). Na^+-loaded melanins exhibit peaks at higher binding energies of 536.46 (NatMel-Na), 535.04 (SynMel-Na), and 535.28 (E-SynMel-Na) eV. These peaks are associated with the formation of sodium carboxylate complexes (COO–Na) (62). Two prominent peaks located near binding energies associated with N

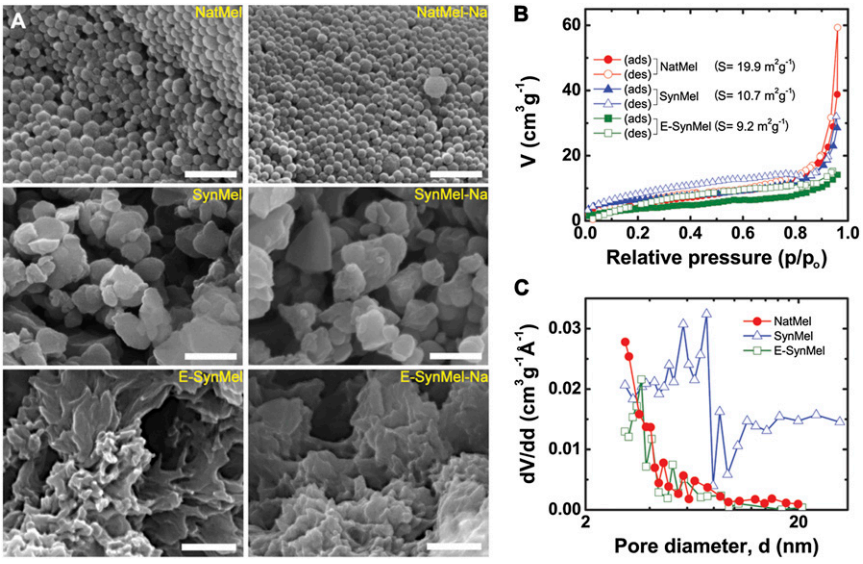

Fig. 1. Structural characterization of eumelanins. (*A*) SEM images of pristine natural (NatMel), Na^+-loaded natural (NatMel-Na), synthetic (SynMel), Na^+-loaded synthetic (SynMel-Na), electro-deposited (E-SynMel), and Na^+-loaded electrodeposited (E-SynMel-Na) melanins. Scale bar, 500 nm. (*B*) Nitrogen adsorption–desorption isotherms and (*C*) pore-size distributions as determined by using the Barrett–Joyner–Halenda method.

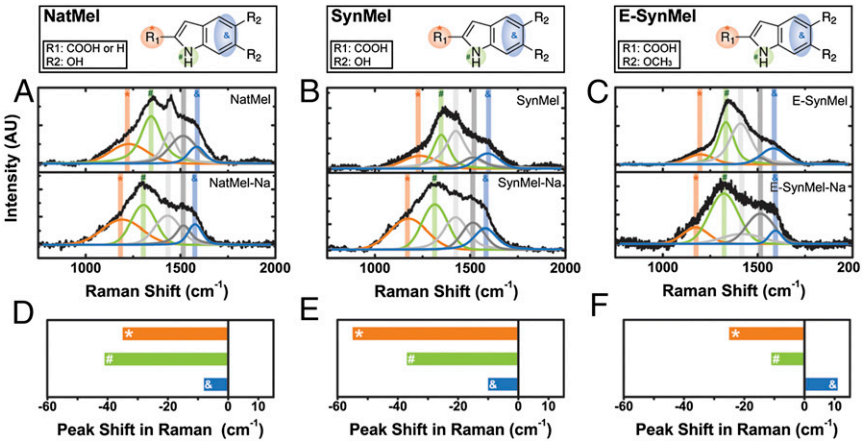

Fig. 2. Raman spectra of eumelanins. (*A*) NatMel and NatMel-Na; (*B*) SynMel and SynMel-Na; (*C*) E-SynMel and E-SynMel-Na. Raw spectra (black lines) are deconvolved into five bands using a Voigt function. The chemical structure of each melanin species is indicated. The functional groups that support Na^+ binding are highlighted in the respective colors. The peak shifts at wavenumbers of 1,220 cm^{-1} (*), 1,341 cm^{-1} (#), and 1,510 cm^{-1} (&) relative to pristine melanin anodes are shown in *D*–*F*. Detailed peak positions and calculated shifts are included in *SI Text* (Table S2).

(1s) are observed at 399.00 ± 0.3 and 397.50 ± 0.4 eV. These peaks can be assigned to aromatic C–N and amine groups (N–H), respectively (64). Peaks centered about 397.50 eV exhibit a larger area under the curve after sodium cation loading. Similar increases in peak area were observed in nitrogen-doped titanium oxide at binding energies that are slightly smaller than 398 eV (65). The overall characteristics of the Raman spectra of pristine NatMel, SynMel, and E-SynMel are comparable to other sp^2-hybridized carbon materials (Fig. 2) (66, 67). Deconvolution using a Voigt function reveals broad peaks between wavenumbers of 1,000 and 1,750 cm^{-1} that are associated with vibrational signatures generated by indole groups. Peaks centered at 1,590 and 1,510 cm^{-1} (blue band) are attributed to stretching vibrations of aromatic C=C and C=N bonds in indole structure. The peak observed at 1,418 cm^{-1} is associated with stretching vibrations in pyrrole-like subunits (67). Two bands at lower wavenumber are observed at 1,220 and 1,341 cm^{-1}. These features correspond to C–OH (orange band) and aromatic C–N groups from indoles (green band), respectively (67). Significant peak shifts are observed in all Na^+-loaded melanin materials. The presence of sodium cations influences the vibrational modes in melanin protomolecules relative to the complementary pristine anode materials (Fig. 2). The largest peak shifts are associated with C–OH and C–N groups, which suggests strong coupling of sodium cations to carboxylic acids and aromatic amines. Similar peak shifts have been observed in boron- and nitrogen-doped single-walled carbon nanotubes and TiO_2 nanoparticles with organic coatings (68).

Sodium-ion loading on melanins was confirmed through thermogravimetric analysis (TGA). Cations coordinate π–π stacking of melanin protomolecules and promote intermolecular hydrogen bonding (69). The TGA profiles of Na^+-loaded NatMel (NatMel-Na) indicate two nodes that occur at 480 and 590 °C (Fig. S4). These data suggest the presence of two distinct populations of bound sodium cations (17, 18). The slope of the plateau between these temperatures suggests that SynMel and E-SynMel are relatively more heterogeneous compared with NatMel (*SI Text*). Na^+-loaded melanins exhibit increased thermal stability compared with pristine melanins for a given composition. These data suggest that cationic species generally stabilize melanin monomers. Thermograms of E-SynMel-Na indicate accelerated mass loss at temperatures above 700 °C compared with pristine E-SynMel. These data suggest that the presence of aryl methoxy groups in E-SynMel may disrupt intermolecular hydrogen bonding (69) and reduce the potential contribution of cationic stabilization and coordination after sodium loading (41, 43).

The electrochemical performance of melanins anodes was characterized by cyclic voltammetry (CV) and galvanostatic half-cell discharge cycles. CV curves of melanins with 1 M Na_2SO_4 electrolyte are shown (Fig. 3). Na^+-loaded melanins collectively exhibit higher peak cathodic currents compared with pristine anodes for all melanin compositions evaluated in this study (Fig. 3 *A*–*C*). Additionally, all Na^+-loaded melanins (Fig. S5) exhibit peak cathodic currents at potentials between 0 and ∼0.2 V (vs. MSE). The redox reactions measured by CV during sodium-ion discharge are largely irreversible. These data suggest that melanin anodes are suitable for primary energy storage materials (70). This operational constraint is fully compatible with envisioned applications in biodegradable and edible medical devices.

The rate of sodium-ion discharge from melanin anodes was also measured using galvanostatic half-cell measurements in aqueous environments with platinum counter electrodes [vs. mercury/mercurous sulfate electrode (MSE)] (Fig. 3 *D*–*F*). Half-cell discharge measurements were initiated from their open-circuit potentials (OCVs) and monitored continuously thereafter. The OCVs of NatMel, SynMel, and E-SynMel were −0.38 ± 0.02, −0.31 ± 0.04, and −0.13 ± 0.04 V, respectively. After sodium cation loading, the OCVs were reduced to −0.73 ± 0.04, −0.73 ± 0.06, and −0.43 ± 0.06 V for NatMel-Na, SynMel-Na, and E-SynMel-Na, respectively. The OCVs of anodes composed of NatMel-Na and SynMel-Na anodes are more negative compared with anodes composed of activated carbon (OCV_{AC} = −0.3 V, Fig. S6) and n-type redox polymers ($OCV_{n\text{-}Poly}$ = −0.6 V) (71, 72). Half-cell discharge profiles of Na^+-loaded melanin anodes exhibit plateaus in potentials between 0 and ∼0.2 V. This consistent feature corresponds to the sodium ion extraction (15, 73, 74). The measurements are in concert with the potential during peak cathodic current as measured by CV (18, 75, 76). Half-cells composed of E-SynMel-Na electrodes exhibit a gradual linear increase in potential (more positive) with a more compressed plateau compared with cells with NatMel and SynMel electrodes. Charge storage capacities measured using a constant discharge rate of 10 mAg^{-1} were 30.4 ± 1.6, 31.1 ± 2.0, and 24.1 ± 2.0 $mAhg^{-1}$ for NatMel-Na, SynMel-Na, and E-SynMel-Na, respectively. Melanin anodes without sodium ions exhibit negligible charge storage capacity. The charge storage capacities of NatMel anodes are comparable to electrodes composed of polyaniline–carbon nanotube composites (12.1 $mAhg^{-1}$) or PPy–carbon fiber electrodes (23.9 $mAhg^{-1}$) and slightly lower compared with the capacities of poly(galvinoxylstyrene) electrodes (42 $mAhg^{-1}$) (72, 77, 78).

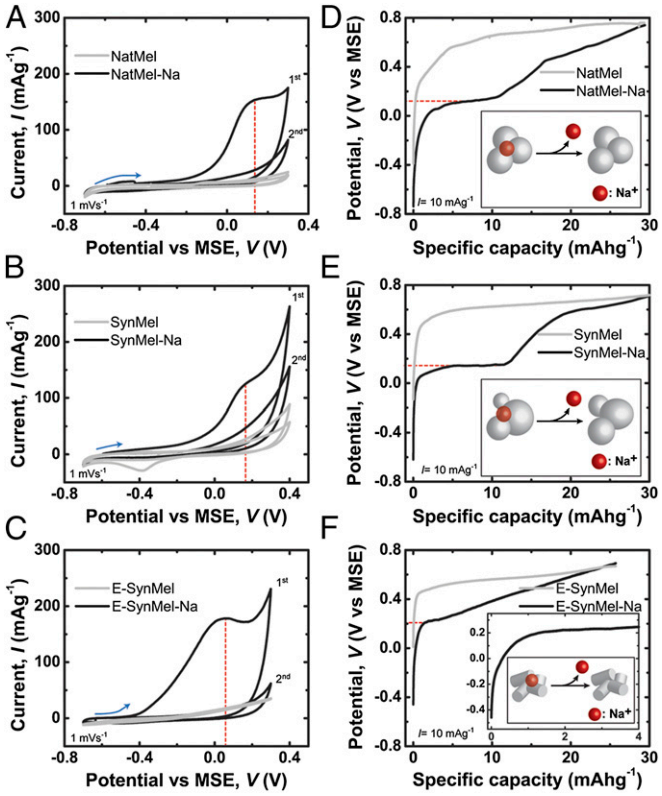

Fig. 3. Electrochemical characterization of eumelanins. (*A–C*) CV of melanins in 1 M Na_2SO_4 electrolyte indicate redox peaks between 0 and ~0.2 V (vs. MSE). Galvanostatic half-cell discharge profiles of melanins at 10 mAg^{-1} measured in 1 M Na_2SO_4 with Pt counter and MSE reference electrodes are shown in *D–F*. Plateaus at potentials of ~0.2 V indicate the release of sodium ions from Na^+-loaded melanin electrodes.

Full cells were prepared using melanin anodes and λ-MnO_2 cathodes (Fig. 4). The initial full cell potentials of NatMel-Na and SynMel-Na were 1.0 V. E-SynMel-Na exhibited a slightly lower potential of 0.7 V due to the higher (more positive) OCV (−0.43 V). The full cell potentials of 1.0 V observed in this work are comparable to other aqueous sodium-ion batteries (14). Galvanostatic discharge profiles were measured using −10 μA. The specific capacities (normalized by anode mass) calculated from discharge profiles of full cells are 16.1 ± 0.8, 12.4 ± 1.2, and 7.9 ± 1.4 $mAhg^{-1}$ ($n = 5$) for NatMel-Na, SynMel-Na, and E-SynMel-Na, respectively. The specific capacities of Na^+-loaded melanin anodes in full cells are approximately 10× higher than corresponding unloaded melanin anodes (Fig. S7 *A–C*). Full cell discharge profiles were measured as a function of the Na^+-loaded melanin anode mass (between 3 and 21 mg; Fig. S7 *D–F*) for a constant λ-MnO_2 cathode mass (8 mg). Specific capacities of λ-MnO_2 cathodes and Na^+-loaded melanin anodes were ~80 and 30 $mAhg^{-1}$, respectively, as measured by half-cell discharge experiments (38). The maximum amount of melanin (21 mg) exhibits a theoretical 1:1 ratio of anode–cathode capacity. These data confirm that the full cell system is anode-limited (79). Full cells composed of λ-MnO_2 cathodes and Na^+-loaded melanin anodes exhibit a specific capacity of 7–16 $mAhg^{-1}$ (normalized by anode mass) over a potential range of 1.0 V. These specific capacities are comparable to other more exotic anode materials used previously in sodium-ion charge storage materials, and are significantly lower than the best-performing materials studied for traditional battery applications (29, 80). However, the envisioned biomedical applications that will be enabled by melanin-based energy storage materials have modest specific capacity requirements that are achievable with the current demonstration.

NatMel-Na anodes exhibit a specific capacity that is 50% larger than SynMel-Na anodes. Two characteristic features likely contribute to the increase (decrease) of charge storage capacity of melanin-based anodes in the full cell system: the presence (absence) of pendant carboxylates and the larger (smaller) surface area. The specific capacities normalized by surface area as measured by BET analysis were 0.79, 1.03, and 0.77 $mAhm^{-2}$ for NatMel-Na, SynMel-Na, and E-SynMel-Na, respectively (Fig. S8*A*). These data highlight the advantageous chemistry of SynMel-Na anodes. Raman spectra further implicate pendant carboxylates as the primary moiety that increases the specific charge storage capacity of SynMel-Na compared with NatMel-Na.

Eumelanin pigments are promising biologically derived anode materials to power transient electronics for use in biomedical applications. A key advantage of melanin-based anodes is the ability to directly use naturally occurring biopolymers with limited postprocessing. Previous examples of biologically derived battery electrodes use polymeric biomaterials as templates that must be functionalized by carbonization (81–83). However, melanins exhibit functional groups and microstructure that permit immediate use of the material as an organic electrode material in aqueous sodium-ion charge storage devices. When used in combination with other biocompatible cathodes, aqueous electrolytes, and sodium ions, melanins could be rapidly used as power supplies for edible or biodegradable electronic medical devices (6, 84). Melanins of natural and synthetic origin are composed of well-characterized monomers. Melanins therefore offer potential regulatory advantages for use in edible electronics compared with alternative exotic synthetic electrode materials, which carry unknown risk. The lifetime of a typical melanin/λ-MnO_2 full cell used in this study is 5 h when operating at discharge rates of 10 μA, which is significantly longer than power supplies that are currently used for ingestible event monitoring devices (85). However, one of the prospective limitations of melanin-based anodes in charge storage devices is the relatively low energy density compared with inorganic electrode materials (14, 15, 86). The performance of melanin anodes in full cells may be further improved by altering

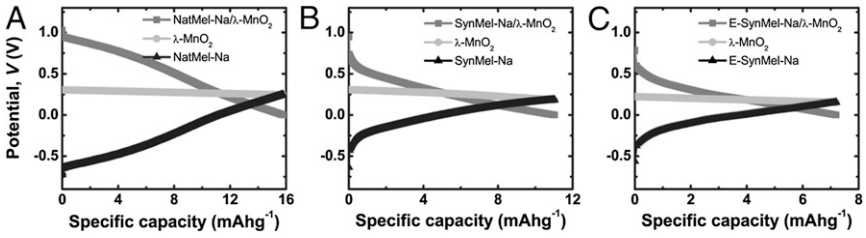

Fig. 4. Potential profiles of full cells are shown using Na^+-loaded melanin anodes and λ-MnO_2 cathodes under discharge rates of -10 μA. Discharges were measured in 1 M Na_2SO_4 wtih Pt counter and reference electrodes. Specific charge storage capacities based on active anode masses were 16.1 ± 0.8, 12.4 ± 1.2, and 7.9 ± 1.4 $mAhg^{-1}$ for (*A*) NatMel-Na, (*B*) SynMel-Na, and (*C*) E-SynMel-Na, respectively ($n = 5$).

the chemical functionality of protomolecules and increasing the surface area through microstructure engineering to maximize the specific sodium-ion loading capacity. These design criteria can be achieved by designing biomimetic materials to control in vitro melanogenesis. Cathodes with higher specific mass densities could also increase the charge storage capacity of full cells. Taken together, the biocompatibility of biologically derived melanin anodes can be used in next-generation biocompatible energy storage systems to power transient biomedical electronics including edible or biodegradable devices.

Materials and Methods

Materials. NatMel (melanin from *S. officinalis*), SynMel (melanin, synthetic), and tetrabutylammonium percholate (TBAP) were purchased from Sigma-Aldrich and used as received. Sodium hydroxide was purchased from Fischer Scientific. DMICA was purchased from Alfa Aesar.

Electrodeposition of Melanin. Electrodeposition of melanin (E-SynMel) was performed by constant current application into conducting substrates in DMICA–acetone solution as previously described (54). Briefly, DMICA (0.01 M) was electrochemically deposited on stainless steels with two-electrode setup using the constant current source (220 programmable current source, Keithley) with a platinum mesh counter electrode (99.9%, 20 × 20 mm, Goodfellow Cambridge Ltd.). E-SynMel was synthesized by depositing DMICA in acetone (>99.5% purity, American Chemical Society reagent grade, Pharmco-Aaper) with TBAP, 99%, Sigma-Aldrich) as counter ions. E-SynMel was deposited using a constant current of 0.4 mA cm^{-2} for 40 min followed by rinsing with acetone. E-SynMel was harvested by mechanical delamination.

Sodium-Ion (Na^+) Loading of Melanin Anodes. Sodium-ion loading was performed by adding pristine melanin (300 mg) to solutions of sodium hydroxide (500 mg, 12.5 mmol) in ethanol (10 mL) at room temperature for 24 h. Excess ethanol (~30 mL) was added to remove unreacted sodium ions. The product was centrifuged to precipitate out the Na^+-loaded melanin while discarding the supernatant. The washing procedure was performed twice for a total of two washes. The precipitate was dried at 100 °C for 1 h in a vacuum oven and stored at ambient conditions.

Spectroscopic and Microscopic Characterization of Melanin Anode Materials. Eumelanin structures were examined by environmental scanning electron microscope (SEM, FEI Quanta 600). Electron dispersive spectroscopy was performed by silicon drift detector (XMAX 80-mm EDX detector, Oxford Instruments). Nitrogen physisorption measurements were performed at 77.3 K using Quadrasorb Si (Quantachrome Instrument). Melanins were degassed at 200 °C for 18 h before BET measurements.

XPS was performed using Kratos Analytical Axis Ultra (Kratos Analytical Ltd.). Survey scan and high-resolution spectra of the 1s orbitals of carbon (C), oxygen (O), and nitrogen (N) were obtained. Elemental analysis was performed using the peak areas and the relative sensitivity factors of the instrumentation to each atomic species. The resulting spectra were analyzed using CasaXPS. Peak fitting was performed with a target of <1.2 eV FWHM in each peak.

Raman spectra were collected using an inverted Raman confocal microscope (inVia Raman microscope, Renishaw) with a 50× objective (Leica Microsystems) and 785-nm-wavelength laser (1.58 eV) over a Raman shift of 700–2,000 cm^{-1}. Five scans with 1 mW of laser power were averaged to minimize sample degradation and maximize the signal-to-noise ratio.

TGA. TGA was conducted by SETSYS Evolution TGA (Setaram Instrumentation) at a heating rate of 3 °C min^{-1} under Ar atmosphere (>99.999%, ultrahigh-purity grade 5.0, Airgas). Melanin samples (~50 mg) were stored in alumina crucibles and degassed with Ar for 6 h before collecting the data from 200 to 1,000 °C.

Preparation and Discharge of Wet-Cell Sodium-Ion Energy Storage. Melanin electrodes were prepared by combining melanin (300 mg) with polytetrafluoroethylene (PTFE, 200–300-μm particle size, Sigma-Aldrich) as a binder in a mass ratio of 75:25. The components of the electrodes were then homogeneously blended using agate mortar and pestle. λ-MnO_2 cathodes were prepared by synthesizing $LiMn_2O_4$ followed by chemical delithiation as previously described (87). Li_2CO_3 was ball milled with electrolytic manganese dioxide (Tronox; Spex 8000, Si_3N_4 crucible) in a stoichiometric molar ratio for 60–120 min. This mixture was pyrolyzed at 750–800 °C in air for 8–12 h. The resultant $LiMn_2O_4$ powder was converted to cubic spinel λ-Mn_2O_4 via acid leaching. Briefly, $LiMn_2O_4$ powder was stirred in 200 mL of 1 M H_2SO_4 solution for 24 h. λ-MnO_2 electrodes were prepared by mixing λ-MnO_2, PTFE, and acetylene black (Alfa Aesar) as conductive additive in a mass ratio of 80:10:10. Electrodes dedicated for electrochemical characterization (melanin = between 3 and 21 mg, λ-MnO_2 = 8 mg) were pressed into stainless steel mesh handling structures (type 304, McMaster-Carr). Discharge lifetimes were measured by monitoring full cell potentials over time and estimated from charge balances. A three-electrode cell was configured with melanin as working electrode against platinum counter electrode and Hg/Hg_2SO_4 (MSE) reference electrode. Multichannel potentiostat–galvanostat (VMP3, Bio-logic) was used to investigate CV and galvanostatic discharge profiles. The apparent (nominal) surface area for disk electrodes was 28.3 mm^2 using a loading of 10 mg m^{-2}. BET surface area was used for all charge storage capacity calculations normalized by area (Fig. S8*A*).

ACKNOWLEDGMENTS. The authors thank Vince Bojan of the Materials Characterization Lab at Pennsylvania State University for assistance in acquiring XPS data. The authors are grateful to Kyu Hun Kim and Youngseok Oh for valuable discussions. The authors acknowledge the financial support provided by the following organizations: American Chemical Society (PRF51980DN17); the Carnegie Mellon University (CMU) School of Engineering; the CMU Center for Technology Transfer and Enterprise Creation; the Pennsylvania Department of Community and Economic Development; Innovation Works (Pittsburgh, PA); the Shurl and Kay Curci Foundation; and the Department of Energy (DE-OE0000226). The authors also thank the CMU Thermomechanical Characterization Facility. NMR instrumentation at CMU was partially supported by National Science Foundation (CHE-0130903 and CHE-1039870).

1. Meredith P, Bettinger CJ, Irimia-Vladu M, Mostert AB, Schwenn PE (2013) Electronic and optoelectronic materials and devices inspired by nature. *Rep Prog Phys* 76(3):034501.
2. Irimia-Vladu M, et al. (2012) Indigo – From jeans to semiconductors: Indigo - A natural pigment for high performance ambipolar organic field effect transistors and circuits. *Adv Mater* 24(3):321–321.
3. Irimia-Vladu M, et al. (2010) Edible electronics: Biocompatible and biodegradable materials for organic field-effect transistors. *Adv Funct Mater* 20(23):4017–4017.
4. Irimia-Vladu M, et al. (2010) Biocompatible and biodegradable materials for organic field-effect transistors. *Adv Funct Mater* 20(23):4069–4076.
5. Hwang S-W, et al. (2013) Materials and fabrication processes for transient and bioresorbable high-performance electronics. *Adv Funct Mater* 23(33):4087–4093.
6. Bettinger CJ, Bao Z (2010) Organic thin-film transistors fabricated on resorbable biomaterial substrates. *Adv Mater* 22(5):651–655.
7. Siegel AC, et al. (2009) Foldable printed circuit boards on paper substrates. *Adv Funct Mater* 20(1):28–35.
8. Bettinger CJ, Bruggeman JP, Misra A, Borenstein JT, Langer R (2009) Biocompatibility of biodegradable semiconducting melanin films for nerve tissue engineering. *Biomaterials* 30(17):3050–3057.
9. Hwang S-W, et al. (2012) A physically transient form of silicon electronics. *Science* 337(6102):1640–1644.
10. Kim D-H, et al. (2011) Epidermal electronics. *Science* 333(6044):838–843.
11. Southcott M, et al. (2013) A pacemaker powered by an implantable biofuel cell operating under conditions mimicking the human blood circulatory system—battery not included. *Phys Chem Chem Phys* 15(17):6278–6283.
12. Wei X, Liu J (2008) Power sources and electrical recharging strategies for implantable medical devices. *Front Energy Power Eng China* 2(1):1–13.
13. Kerzenmacher S, Ducree J, Zengerle R, von Stetten F (2008) An abiotically catalyzed glucose fuel cell for powering medical implants: Reconstructed manufacturing protocol and analysis of performance. *J Power Sources* 182(1):66–75.
14. Li Z, Young D, Xiang K, Carter WC, Chiang Y-M (2013) Towards high power high energy aqueous sodium-ion batteries: The $NaTi_2(PO_4)_3/Na_{0.44}MnO_2$ system. *Adv Energy Mater* 3(3):290–294.
15. Wu W, Mohamed A, Whitacre JF (2013) Microwave synthesized $NaTi_2(PO_4)_3$ as an aqueous sodium-ion negative electrode. *J Electrochem Soc* 160(3):A497–A504.
16. Kim YJ, Chun S-E, Whitacre J, Bettinger CJ (2013) Self-deployable current sources fabricated from edible materials. *J Mater Chem B* 1(31):3781–3788.
17. Park Y, et al. (2012) Sodium terephthalate as an organic anode material for sodium ion batteries. *Adv Mater* 24(26):3562–3567.
18. Armand M, et al. (2009) Conjugated dicarboxylate anodes for Li-ion batteries. *Nat Mater* 8(2):120–125.
19. Renault S, Geng J, Dolhem F, Poizot P (2011) Evaluation of polyketones with N-cyclic structure as electrode material for electrochemical energy storage: Case of pyromellitic diimide dilithium salt. *Chem Commun (Camb)* 47(8):2414–2416.
20. Chen H, et al. (2008) From biomass to a renewable $LixC_6O_6$ organic electrode for sustainable Li-ion batteries. *ChemSusChem* 1(4):348–355.
21. Reddy ALM, et al. (2012) Lithium storage mechanisms in purpurin based organic lithium ion battery electrodes. *Sci Rep* 2:960.

22. Kettlgruber G, et al. (2013) Intrinsically stretchable and rechargeable batteries for self-powered stretchable electronics. *J Mater Chem A* 1(18):5505–5508.
23. Hu L, et al. (2010) Stretchable, porous, and conductive energy textiles. *Nano Lett* 10(2):708–714.
24. Gaikwad AM, et al. (2012) Highly stretchable alkaline batteries based on an embedded conductive fabric. *Adv Mater* 24(37):5071–5076.
25. Wang C, Zheng W, Yue Z, Too CO, Wallace GG (2011) Buckled, stretchable polypyrrole electrodes for battery applications. *Adv Mater* 23(31):3580–3584.
26. Sakaushi K, et al. (2013) Aromatic porous-honeycomb electrodes for a sodium-organic energy storage device. *Nat Commun* 4:1485.
27. Gaikwad AM, Whiting GL, Steingart DA, Arias AC (2011) Highly flexible, printed alkaline batteries based on mesh-embedded electrodes. *Adv Mater* 23(29):3251–3255.
28. Chen Z, et al. (2012) High-performance sodium-ion pseudocapacitors based on hierarchically porous nanowire composites. *ACS Nano* 6(5):4319–4327.
29. Mai L, et al. (2013) Fast ionic diffusion-enabled nanoflake electrode by spontaneous electrochemical pre-intercalation for high-performance supercapacitor. *Sci Rep* 3:1718.
30. Palomares V, et al. (2012) Na-ion batteries, recent advances and present challenges to become low cost energy storage systems. *Energ Environ Sci* 5(3):5884–5901.
31. Yang L, Liu L, Zhu Y, Wang X, Wu Y (2012) Preparation of carbon coated MoO_2 nanobelts and their high performance as anode materials for lithium ion batteries. *J Mater Chem* 22(26):13148–13152.
32. Kim J, Yun S, Ounaies Z (2006) Discovery of cellulose as a smart material. *Macromolecules* 39(12):4202–4206.
33. Milczarek G, Inganäs O (2012) Renewable cathode materials from biopolymer/conjugated polymer interpenetrating networks. *Science* 335(6075):1468–1471.
34. Yang C, Liu P (2009) Water-dispersed conductive polypyrroles doped with lignosulfonate and the weak temperature dependence of electrical conductivity. *Ind Eng Chem Res* 48(21):9498–9503.
35. Li Z, et al. (2013) Mesoporous nitrogen-rich carbons derived from protein for ultra-high capacity battery anodes and supercapacitors. *Energ Environ Sci* 6(3):871–878.
36. Wang L, Wang D, Zhang F-X, Jin J (2013) Protein-inspired synthesis of SnO_2 nanocrystals with controlled carbon nanocoating as anode materials for lithium-ion battery. *RSC Advances* 3(5):1307–1310.
37. Ajayi FF, Weigele PR (2012) A terracotta bio-battery. *Bioresour Technol* 116(0):86–91.
38. Whitacre JF, et al. (2012) An aqueous electrolyte, sodium ion functional, large format energy storage device for stationary applications. *J Power Sources* 213(0):255–264.
39. Mostert AB, et al. (2012) Role of semiconductivity and ion transport in the electrical conduction of melanin. *Proc Natl Acad Sci USA* 109(23):8943–8947.
40. d'Ischia M, Napolitano A, Pezzella A, Meredith P, Sarna T (2009) Chemical and structural diversity in eumelanins: Unexplored bio-optoelectronic materials. *Angew Chem Int Ed Engl* 48(22):3914–3921.
41. Meredith P, Sarna T (2006) The physical and chemical properties of eumelanin. *Pigment Cell Res* 19(6):572–594.
42. Simon JD, Peles D, Wakamatsu K, Ito S (2009) Current challenges in understanding melanogenesis: Bridging chemistry, biological control, morphology, and function. *Pigment Cell Melanoma Res* 22(5):563–579.
43. Hong L, Simon JD (2007) Current understanding of the binding sites, capacity, affinity, and biological significance of metals in melanin. *J Phys Chem B* 111(28):7938–7947.
44. Hong L, Simon JD (2006) Insight into the binding of divalent cations to Sepia eumelanin from IR absorption spectroscopy. *Photochem Photobiol* 82(5):1265–1269.
45. Eisenman HC, Casadevall A (2012) Synthesis and assembly of fungal melanin. *Appl Microbiol Biotechnol* 93(3):931–940.
46. Wakamatsu K, Nakanishi Y, Miyazaki N, Kolbe L, Ito S (2012) UVA-induced oxidative degradation of melanins: Fission of indole moiety in eumelanin and conversion to benzothiazole moiety in pheomelanin. *Pigment Cell Melanoma Res* 25(4):434–445.
47. Watt AAR, Bothma JP, Meredith P (2009) The supramolecular structure of melanin. *Soft Matter* 5(19):3754–3760.
48. Meng S, Kaxiras E (2008) Theoretical models of eumelanin protomolecules and their optical properties. *Biophys J* 94(6):2095–2105.
49. Sangaletti L, et al. (2009) Polymerization effects and localized electronic states in condensed-phase eumelanin. *Phys Rev B* 80(17):174203.
50. Kaxiras E, Tsolakidis A, Zonios G, Meng S (2006) Structural model of eumelanin. *Phys Rev Lett* 97(21):218102.
51. Chen C-T, et al. (2013) Self-assembly of tetramers of 5,6-dihydroxyindole explains the primary physical properties of eumelanin: Experiment, simulation, and design. *ACS Nano* 7(2):1524–1532.
52. Kim IG, Nam HJ, Ahn HJ, Jung D-Y (2011) Electrochemical growth of synthetic melanin thin films by constant potential methods. *Electrochim Acta* 56(7):2954–2959.
53. Belitsky JM, Ellowitz MZ, Lye D, Kilbo AL (2012) Small molecule modulators of aggregation in synthetic melanin polymerizations. *Bioorg Med Chem Lett* 22(17):5503–5507.
54. Povlich LK, Le J, Kim J, Martin DC (2010) Poly(5,6-dimethoxyindole-2-carboxylic acid) (PDMICA): A melanin-like polymer with unique electrochromic and structural properties. *Macromolecules* 43(8):3770–3774.
55. Wang HG, et al. (2013) Nitrogen-doped porous carbon nanosheets as low-cost, high-performance anode material for sodium-ion batteries. *ChemSusChem* 6(1):56–60.
56. Collins J, Ngo T, Qu D, Foster M (2013) Spectroscopic investigations of sequential nitric acid treatments on granulated activated carbon: Effects of surface oxygen groups on p density. *Carbon* 57(0):174–183.
57. Sing KSW, et al. (1985) Reporting physisorption data for gas/solid systems with special reference to the determination of surface area and porosity. *Pure Appl Chem* 57(4): 603–619.
58. Holten-Andersen N, et al. (2011) pH-induced metal-ligand cross-links inspired by mussel yield self-healing polymer networks with near-covalent elastic moduli. *Proc Natl Acad Sci USA* 108(7):2651–2655.
59. Hong L, Liu Y, Simon JD (2004) Binding of metal ions to melanin and their effects on the aerobic reactivity. *Photochem Photobiol* 80(3):477–481.
60. Najder-Kozdrowska L, Pilawa B, Wieckowski AB, Buszman E, Wrzesniok D (2009) Influence of copper(II) ions on radicals in DOPA-melanin. *Appl Magn Reson* 36(1):81–88.
61. Lindgren J, et al. (2012) Molecular preservation of the pigment melanin in fossil melanosomes. *Nat Commun* 3:824.
62. Balazs DJ, et al. (2004) Inhibition of bacterial adhesion on PVC endotracheal tubes by RF-oxygen glow discharge, sodium hydroxide and silver nitrate treatments. *Biomaterials* 25(11):2139–2151.
63. Nethravathi C, Anumol EA, Rajamathi M, Ravishankar N (2011) Highly dispersed ultrafine Pt and PtRu nanoparticles on graphene: Formation mechanism and electrocatalytic activity. *Nanoscale* 3(2):569–571.
64. Zhang K, Zhang LL, Zhao XS, Wu J (2010) Graphene/polyaniline nanofiber composites as supercapacitor electrodes. *Chem Mater* 22(4):1392–1401.
65. Popa M, et al. (2010) Synthesis and structural characteristics of nitrogen doped TiO_2 aerogels. *Microporous Mesoporous Mater* 132(1–2):80–86.
66. Capozzi V, et al. (2005) Raman and optical spectroscopy of eumelanin films. *J Mol Struct* 744-747(0):717–721.
67. Centeno SA, Shamir J (2008) Surface enhanced Raman scattering (SERS) and FTIR characterization of the sepia melanin pigment used in works of art. *J Mol Struct* 873(1-3):149–159.
68. Suzuki S, Hibino H (2011) Characterization of doped single-wall carbon nanotubes by Raman spectroscopy. *Carbon* 49(7):2264–2272.
69. Glowacki ED, Irimia-Vladu M, Bauer S, Sariciftci NS (2013) Hydrogen bonds in molecular solids - from biological systems to organic electronics. *J Mater Chem B* 1(31): 3742–3753.
70. Wei D, et al. (2012) Graphene from electrochemical exfoliation and its direct applications in enhanced energy storage devices. *Chem Commun (Camb)* 48(9):1239–1241.
71. Janoschka T, Hager MD, Schubert US (2012) Powering up the future: Radical polymers for battery applications. *Adv Mater* 24(48):6397–6409.
72. Suga T, Sugita S, Ohshiro H, Oyaizu K, Nishide H (2011) p- and n-Type bipolar redox-active radical polymer: Toward totally organic polymer-based rechargeable devices with variable configuration. *Adv Mater* 23(6):751–754.
73. Moreau P, Guyomard D, Gaubicher J, Boucher F (2010) Structure and stability of sodium intercalated phases in olivine $FePO_4$. *Chem Mater* 22(14):4126–4128.
74. Lee KT, Ramesh TN, Nan F, Botton G, Nazar LF (2011) Topochemical synthesis of sodium metal phosphate olivines for sodium-ion batteries. *Chem Mater* 23(16): 3593–3600.
75. Wessells CD, Peddada SV, Huggins RA, Cui Y (2011) Nickel hexacyanoferrate nanoparticle electrodes for aqueous sodium and potassium ion batteries. *Nano Lett* 11(12): 5421–5425.
76. Chen H, et al. (2009) Lithium salt of tetrahydroxybenzoquinone: Toward the development of a sustainable Li-ion battery. *J Am Chem Soc* 131(25):8984–8988.
77. Wang CY, Mottaghitalab V, Too CO, Spinks GM, Wallace GG (2007) Polyaniline and polyaniline-carbon nanotube composite fibres as battery materials in ionic liquid electrolyte. *J Power Sources* 163(2):1105–1109.
78. Rudge A, Davey J, Raistrick I, Gottesfeld S, Ferraris JP (1994) Conducting polymers as active materials in electrochemical capacitors. *J Power Sources* 47(1-2):89–107.
79. Whitacre JF, Tevar A, Sharma S (2010) Na4Mn9O18 as a positive electrode material for an aqueous electrolyte sodium-ion energy storage device. *Electrochem Commun* 12(3):463–466.
80. Lang X, Hirata A, Fujita T, Chen M (2011) Nanoporous metal/oxide hybrid electrodes for electrochemical supercapacitors. *Nat Nanotechnol* 6(4):232–236.
81. Marsh H, Reinoso FR (2006) *Activated Carbon* (Elsevier, Amsterdam).
82. Hu B, et al. (2010) Engineering carbon materials from the hydrothermal carbonization process of biomass. *Adv Mater* 22(7):813–828.
83. Cheng F, Liang J, Tao Z, Chen J (2011) Functional materials for rechargeable batteries. *Adv Mater* 23(15):1695–1715.
84. Muskovich M, Bettinger CJ (2012) Biomaterials-based electronics: polymers and interfaces for biology and medicine. *Adv Healthc Mater* 1(3):248–266.
85. Robertson T, et al. (2010) US Patent 2010/0185055 A1.
86. Slater MD, Kim D, Lee E, Johnson CS (2012) Sodium-ion batteries. *Adv Funct Mater* 23(8):947–958.
87. Chun S-E, Picard YN, Whitacre JF (2011) Relating precursor pyrolysis conditions and aqueous electrolyte capacitive energy storage properties for activated carbons derived from anhydrous glucose-d. *J Electrochem Soc* 158(2):A83–A92.